Supplementary information for

A Disordered–Ordered TiO_2/TiO_{2-x} Homostructure Hosting a High-Mobility Interfacial Conductive Layer for Robust Symmetric Rectification

Yunyun Li[1,2], Chenglin Li[3], Lei Wang[2], Zhuoyuan Li[2], Yuqing Zhu[2], Diwen Zhou[2,*], Guoming Lin[2,*], Weiguang Lan[2,3], Yuanwei Lin[4,5,*]

[1] Fujian Provincial Key Laboratory of Ecology-Toxicological Effects & Control for Emerging Contaminants, Key Laboratory of Ecological Environment and Information Atlas, College of Environmental and Biological Engineering, Putian University, Putian 351100, China

[2] State Key Laboratory of Green and Efficient Development of Phosphorus Resources & School of Future Technology, Fuzhou 350108, China

[3] Department of Chemistry & Faculty of Science, National University of Singapore, 119077, Singapore.

[4] Beijing National Laboratory for Molecular Sciences, State Key Laboratory for Structural Chemistry of Unstable and Stable Species, College of Chemistry and Molecular Engineering, Peking University, Beijing, 100871, China.

[5] Center for Nanoscience and Nanotechnology, Academy for Advanced Interdisciplinary Studies, Peking University, Beijing, 100871, China.

[*]Email: diwenzhou@fzu.edu.cn (D.Z.); linguoming@fzu.edu.cn (G.L.); yuanweilin@pku.edu.cn (Y.L.)

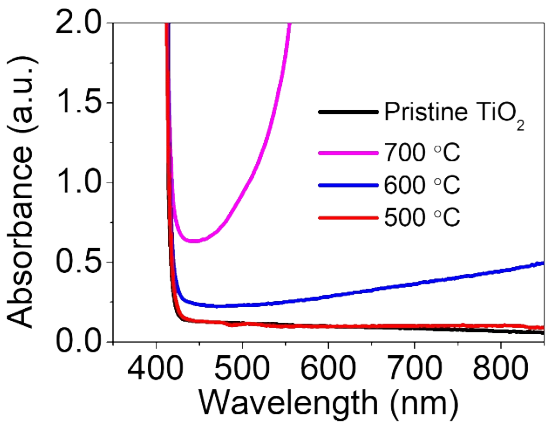

Figure S1. UV–vis absorption evolution of rutile TiO_2 single crystals after CVR in H_2 at 500, 600, and 700 °C for 2 h.

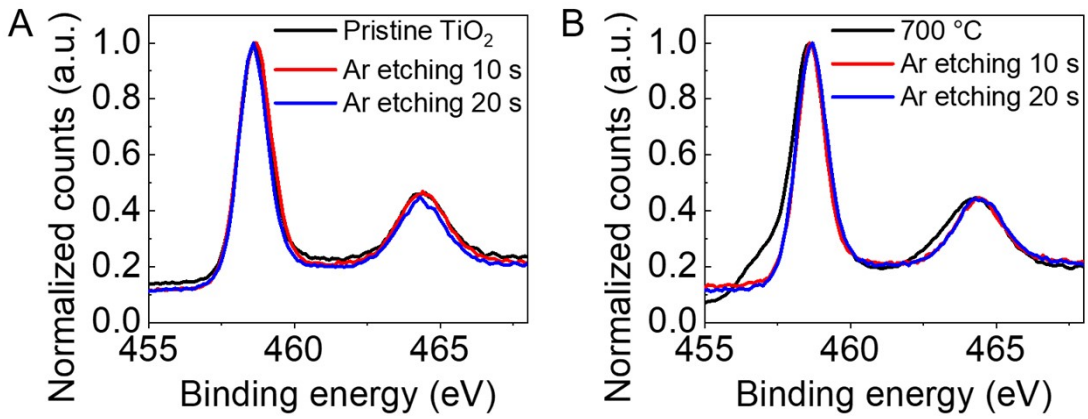

Figure S2. Ti 2p XPS spectra collected before and after Ar-ion etching. (A) Comparison of pristine TiO_2 measured at the surface and after Ar etching for 10 and 20 s. (B) Comparison of the 700 °C-treated TiO_{2-x} sample measured at the surface and after Ar etching for 10 and 20 s.

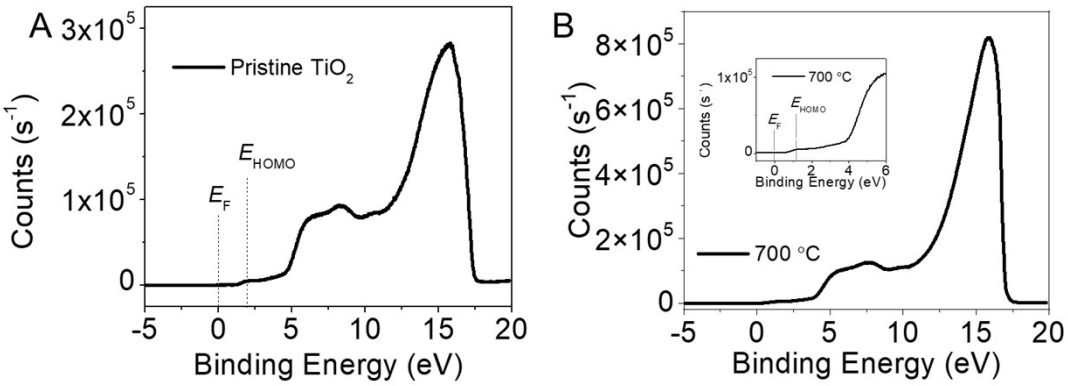

Figure S3. Ultraviolet photoelectronic spectra of the samples treated by CVD at different temperatures. (A) Pristine rutile crystal. (B) Crystal treated by 700 °C, Inset: enlarged view of the low binding energy area.

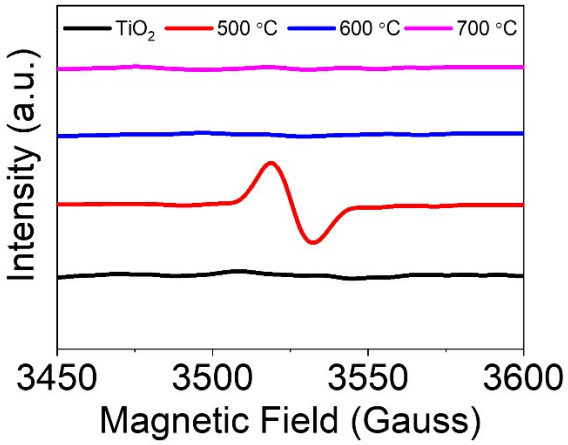

Figure S4. Electron paramagnetic resonance spectra of the samples.

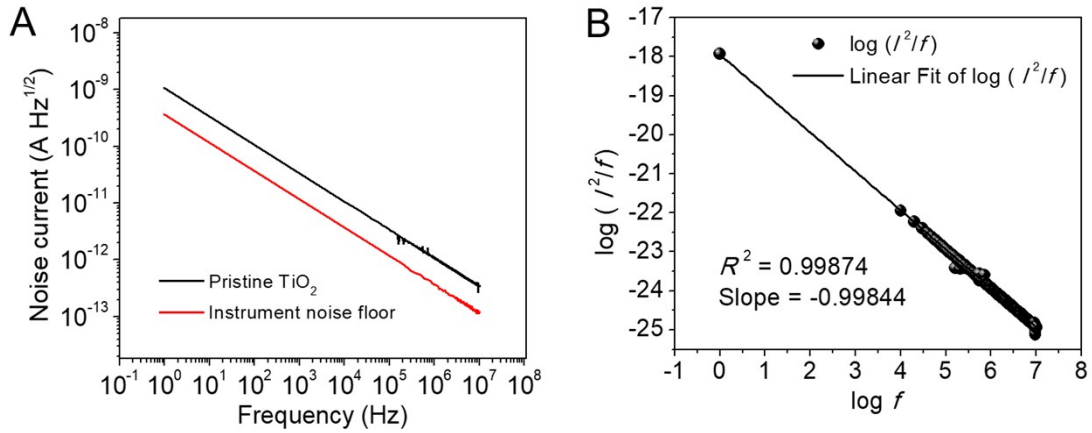

Figure S5. Locked-in amplifier characterization of the rutile crystal device. (A) Frequency dependent noise current of the device based on pristine TiO_2 single crystal treated at 500 °C. (B) Linear fit of the noise current shown in (A).

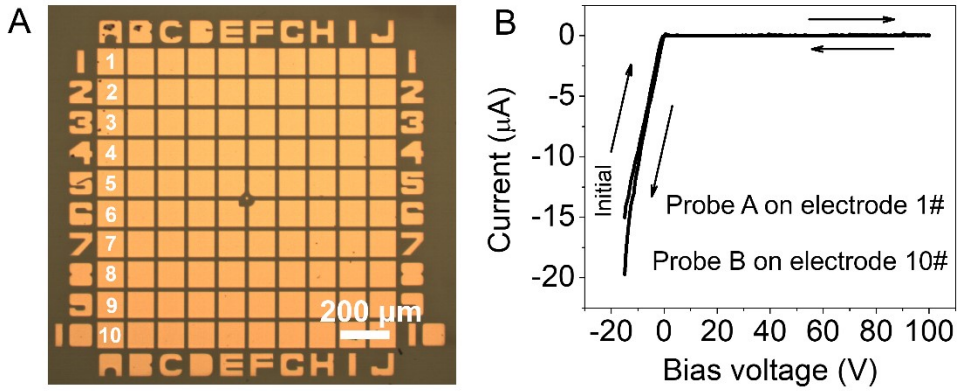

Figure S6. Investigation of the reserve breakdown voltage. (A) Optical image of the rectifying diodes array. (B) *I-V* curve of the rectifying diode with probe A and B put on electrode 1# and 10#, respectively.

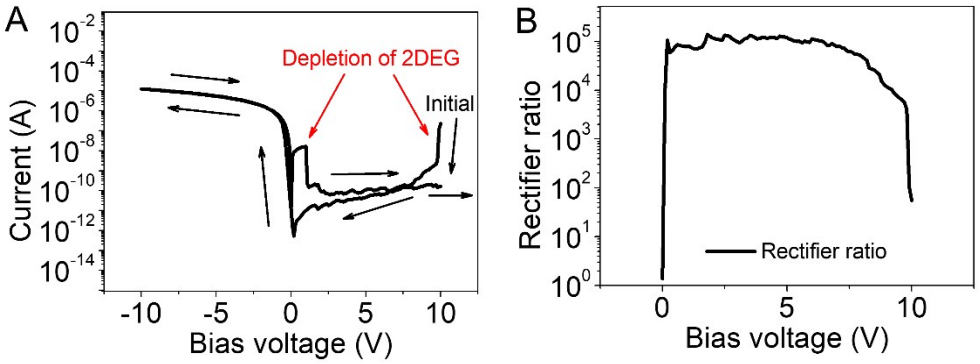

Figure S7. Device performances with sweeping range of ±10 V. (**A**) *I-V* curve of the rectifying diode plot on logarithmic coordinates presenting the depletion of 2DEG. (**B**) Bias voltage dependent rectifier ratio of the device.

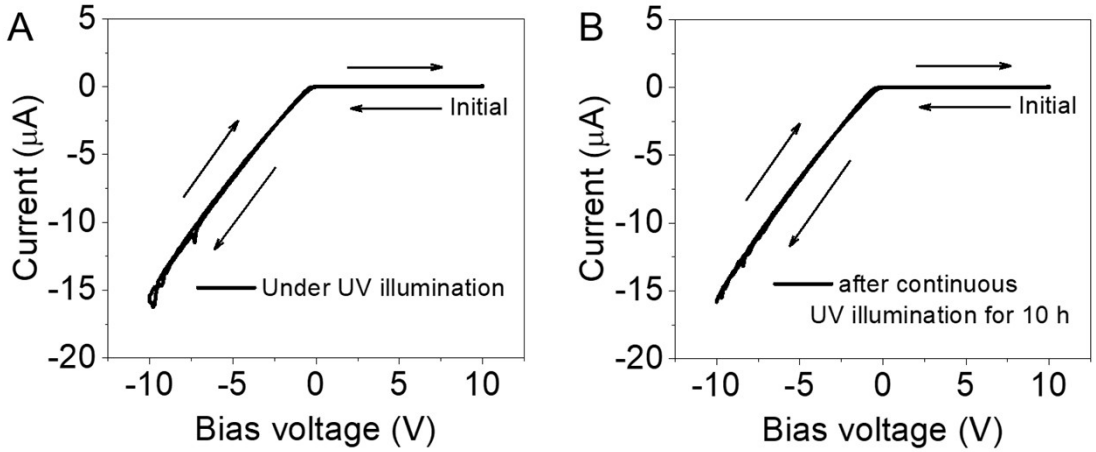

Figure S8. *I-V* curves of the rectifying diodes (A) under UV illumination and (B) after continuous UV illumination for 10 h. The illumination intensity was approximately 50 mW cm^{-2}, and the wavelength was 365 nm.

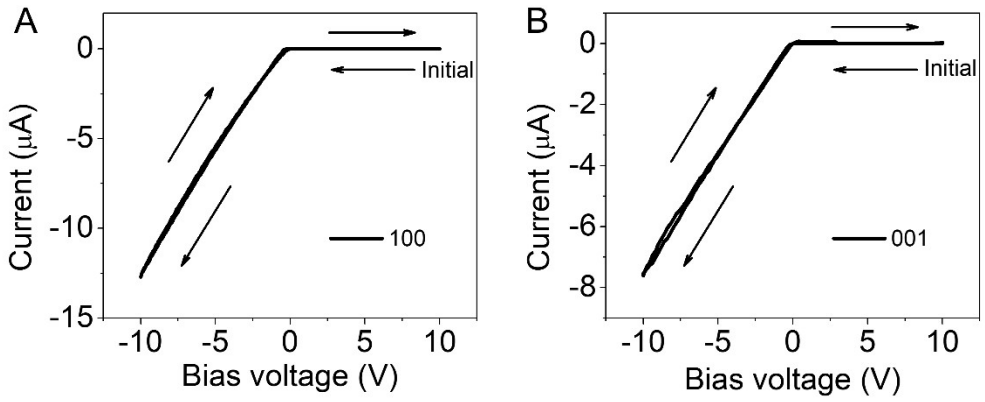

Figure S9. *I-V* curves of the rectifying diodes from (A) (100), and (B) (001) facet.

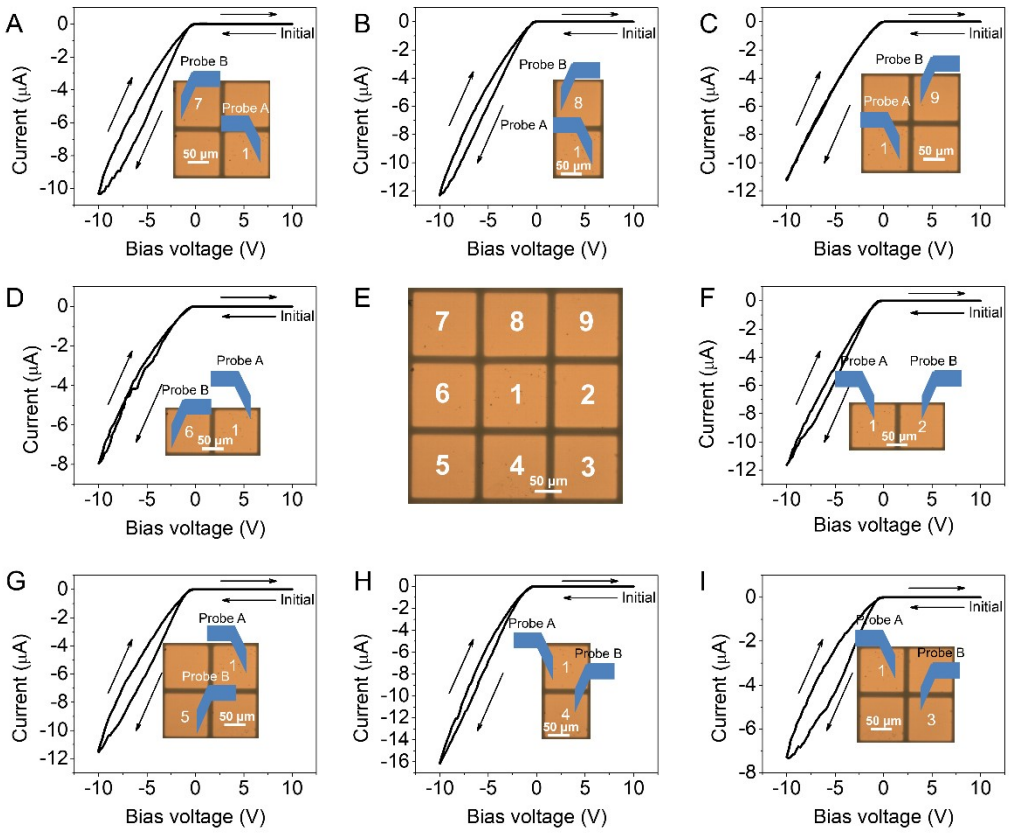

Figure 10. *I-V* curves of the rectifying diode array from different sample orientations. Probe A is set to be put on electrode 1#, and sweeping direction is set to be from reverse to forward. A-D, (A) Probe B on electrode 7#, (B) Probe B on electrode 8#, (C) Probe B on electrode 9#, (D) Probe B on electrode 6#. (E) Optical image of the rectifying diode array. F-I, (F) Probe B on electrode 2#, (G) Probe B on electrode 5#, (H) Probe B on electrode 4#, (I) Probe B on electrode 3#.

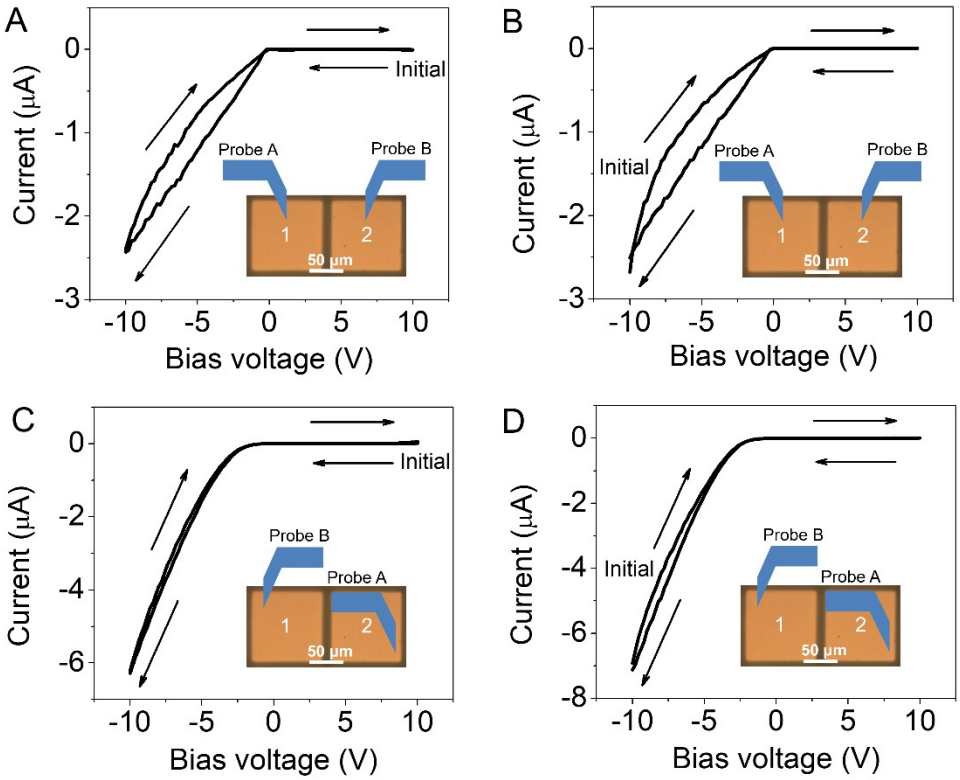

Figure S11. *I-V* curves of the same rectifying diode from different sample orientations and sweeping directions. (A) Probe A on electrode 1#, probe B on electrode 2#, sweeping from reverse to forward. (B) Probe A on electrode 1#, probe B on electrode 2#, sweeping from forward to reverse. (C) Probe A on electrode 2#, probe B on electrode 1#, sweeping from reverse to forward. (D) Probe A on electrode 2#, probe B on electrode 1#, sweeping from forward to reverse.

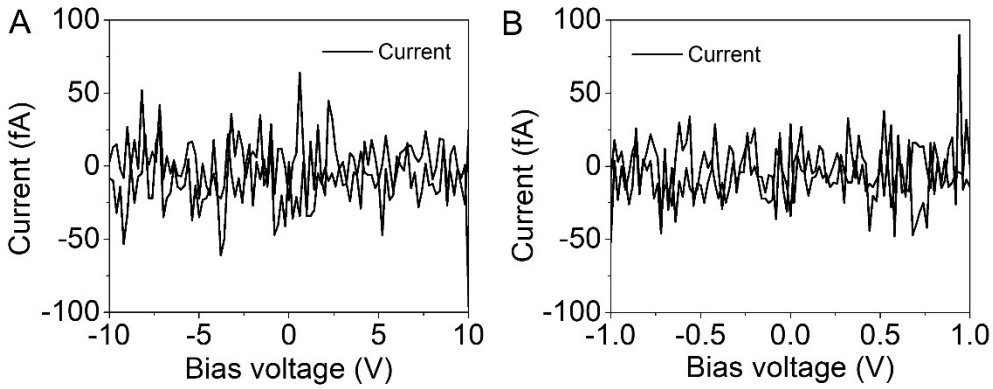

Figure S12. Control experiments of the device based on pristine rutile crystal. (A) Sweeping back and forth between 10 V and -10 V. (B) Sweeping back and forth between 1 V and -1 V.

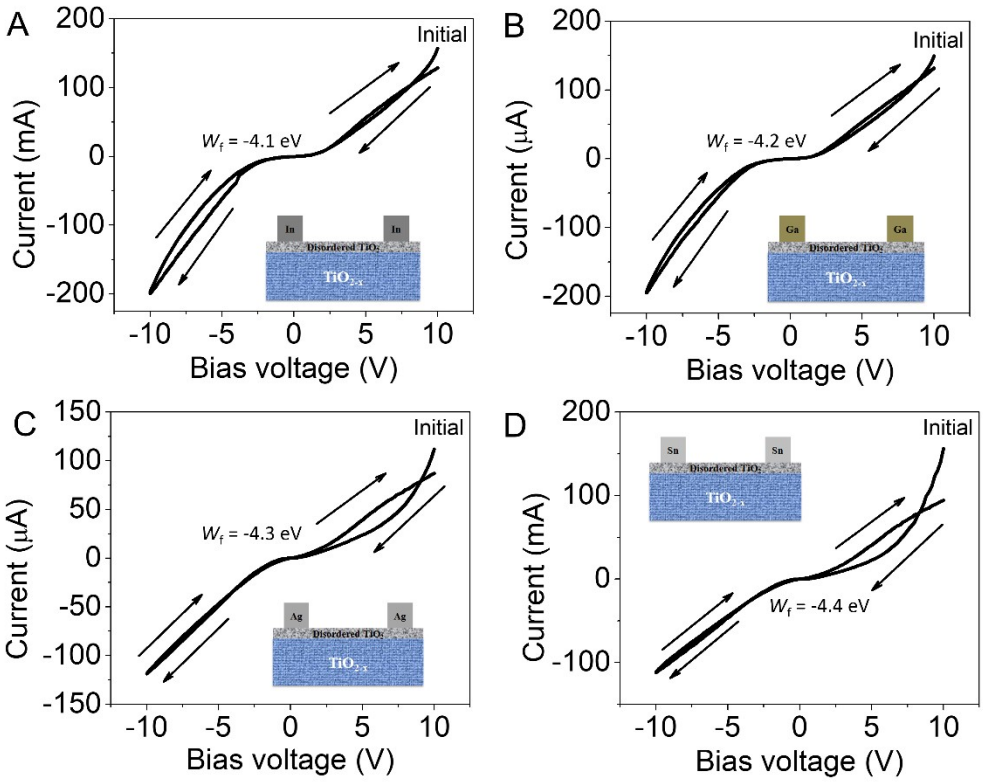

Figure S13. *I-V* curves the devices with (A) Indium, (B) Gallium, (C) Silver, and (D) Tin electrode, respectively. Inset: schematic illustration of the device configurations.

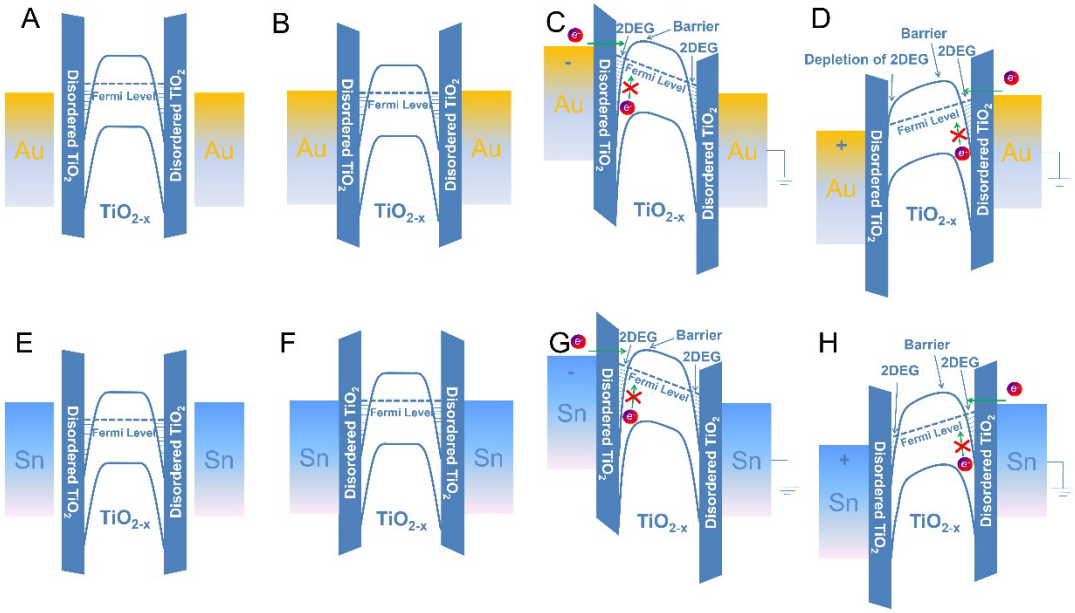

Figure S14. (A-D) Mechanism of the working device based on gold electrode. (E-H) Mechanism of the control device based on tin electrode.